



HAL
open science

Modeling and numerical study of the influence of imperfect interface properties on the reflection coefficient for isotropic multilayered structures.

A Loukkal, M Lematre, Maxime Bavencoffe, M Lethiecq

► To cite this version:

A Loukkal, M Lematre, Maxime Bavencoffe, M Lethiecq. Modeling and numerical study of the influence of imperfect interface properties on the reflection coefficient for isotropic multilayered structures.. Ultrasonics, 2020, 103, pp.106099. 10.1016/j.ultras.2020.106099 . hal-03018520

HAL Id: hal-03018520

<https://hal.science/hal-03018520>

Submitted on 7 Mar 2022

HAL is a multi-disciplinary open access archive for the deposit and dissemination of scientific research documents, whether they are published or not. The documents may come from teaching and research institutions in France or abroad, or from public or private research centers.

L'archive ouverte pluridisciplinaire **HAL**, est destinée au dépôt et à la diffusion de documents scientifiques de niveau recherche, publiés ou non, émanant des établissements d'enseignement et de recherche français ou étrangers, des laboratoires publics ou privés.



Distributed under a Creative Commons Attribution - NonCommercial 4.0 International License

Modeling and numerical study of the influence of imperfect interface properties on the reflection coefficient for isotropic multilayered structures

A.Loukkal^{1*}, M.Lematre¹, M.Bavencoffe¹, M.Lethiecq¹

¹GREMAN UMR 7347, Université de Tours, INSA Centre Val de Loire, 3 rue de la
Chocolaterie, Blois, France
abderrahmane.loukkal@univ-tours.fr

Abstract

The microelectronics industry is expressing an increased demand for the development of non-destructive tools and methods for health control and diagnostics in multilayered structures. The purpose of these tools is to detect problems such as delaminations, inclusions and microcracks. The aim of this paper is to study the effect of imperfect interfaces on the wave propagation in multilayered structures. This type of structure represents the typical architecture of many microelectronic components. This study will be based on the calculation of the reflection coefficient and the guided waves dispersion curves. The investigated structure is an isotropic trilayer where two metallic layers are bonded together by an adhesive layer made of an epoxy resin. Comparisons were performed in order to evaluate numerically the influence of several properties of the adhesive layer on the guided waves behavior. In addition, an imperfect viscoelastic interface layer model [1] has been implemented in order to simulate different adherence qualities between the metallic layers.

Keywords: reflection coefficient; multilayer; imperfect interface; guided waves; dispersion curves; $V(z,f)$ method; modeling.

1. Introduction

The need for monitoring the structural health of multilayered components in the microelectronics industry has driven the development of nondestructive techniques to characterize their integrity. Therefore, a reliable nondestructive method to evaluate the interface quality is of great utility.

Models assessing the adhesion quality between two solids have already been developed [2–5]. Rokhlin *et al.*[1,6] established imperfect interface analytical models based on an interfacial layer, located between two substrates, whose thickness is much smaller than the wavelength in the interface medium. Furthermore, theoretical and numerical analysis have been performed to describe the wave interaction with imperfect interlayer interfaces using spring boundary conditions [2,7–9]. The interfacial soundness can therefore be characterized by the normal and shear stiffnesses of the modeled interface. In order to obtain these interfacial stiffnesses, procedures addressing the amplitude reflection or transmission coefficients of bulk ultrasonic waves have been proposed [10–13].

Studies on guided waves in multilayered structures have also been conducted in order to investigate the interfacial areas [14–21]. In [16], the authors studied numerically and experimentally the impact of different interfacial conditions on the ultrasonic guided waves propagation in multilayered structures. They came to the conclusion that for particular frequency ranges and values of applied stress the velocity of the S0 mode is affected by the interfacial conditions.

The viscoelastic interface layer model established by Rokhlin *et al.*[1] was applied in the case of two isotropic half spaces bounded together. In this work, the same viscoelastic model is used, but implemented in the modeling of the reflection coefficient of a multilayered structure. This study is included in the frame of $V(z)$ measurements in order to characterize adherence properties in multilayered structures. When inverting the $V(z, f)$ experimental data, it allows to rebuild the reflection coefficient with respect to the incidence angle and frequency $R(\theta, f)$ with a simple experimental set-up, that works in normal incidence only, with the use of a forward transducer of large angular aperture. The guided modes of the structure are sensitive to the interface conditions between layers, for this, each guided mode needs to be isolated. Thus, the reflection coefficient is used in this study as a parameter of control since it gives the resonance modes which are shown to correspond to the guided modes of the structure. In addition, the study of the reflection coefficient avoids the difficulty in guided waves measurements, thanks to the $V(z, f)$ method as previously described. The aim of this paper is, thus,

to study the effect of the degradation of the boundary conditions, relative to an adhesive joint, on the reflection coefficient magnitude and the corresponding guided waves behavior.

This paper is structured as follows: in Section 2, the theoretical background, based on the transfer matrix method [22] and the viscoelastic interface layer, is described. The pertinence of the comparison of the minima of the reflection coefficient obtained for a trilayer immersed in water with the guided waves dispersion curves in vacuum is established in Section 3. In the same Section, the waves coupling phenomenon between the different layers is highlighted. Section 4 presents studies of the influence of the different parameters of the adhesive joint.

2. Theoretical background

An isotropic multilayered structure consisting of N layers is considered (Figure 1). Each layer k of this structure has a thickness d_k and the total thickness is equal to D . The multilayer structure is immersed in water (media 0 and $N + 1$) and a longitudinal wave is assumed to be incident on the structure with an angle θ_0 .

The displacements and stresses existing at the bottom of a layer are connected to those at the top of the same layer by means of a layer transfer matrix as described in relation (1).

$$\begin{pmatrix} u_1 \\ u_3 \\ \sigma_{33} \\ \sigma_{13} \end{pmatrix} = B \begin{pmatrix} u_1' \\ u_3' \\ \sigma_{33}' \\ \sigma_{13}' \end{pmatrix} \quad (1)$$

where u_1 , u_3 and u_1' , u_3' are respectively the horizontal and vertical components of the displacements of the lower and the upper face of a layer. B is the 4*4 layer transfer matrix.

The continuity conditions then make it possible to establish a global transfer matrix resulting from the product of the transfer matrices of the successive layers. This global matrix allows the displacements and stresses of the top layer to be related to those of the bottom one as follows:

$$T = \left\{ \prod_{k=N}^{k=1} I_k B_k \right\} I_0 \quad (2)$$

where T is the global transfer matrix of the multilayered structure, I_k is the interface matrix relating the displacements and stresses of the consecutive layers. B_k is the local transfer matrix of layer k and I_0 is the interface matrix relating the displacements and stresses of the upper layer of the multilayer to those existing in the coupling fluid (water in this case).

In the model, imperfect interfaces are modeled by an interfacial layer. The latter possesses a thickness much smaller than those of the other layers of the structure. The imperfect interface layer has been modeled by a viscoelastic material whose properties vary according to its structure [1]. This virtual material obeys to the Maxwell model. Such a material is represented as a series association of a hookean spring and a purely viscous damper. The viscoelasticity is described by an imaginary component in the elastic coefficients of the material constituting the interface layer.

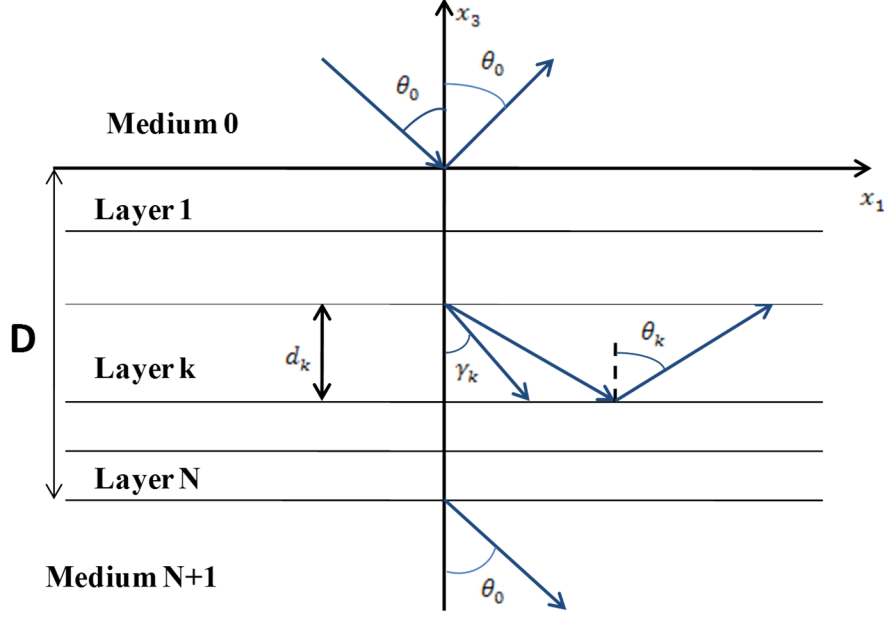


Figure 1: Multilayered structure geometry

Thus, the bulk modulus and the shear modulus of the interfacial layer are respectively:

$$K = K_0 + (K_\infty - K_0) \left(\frac{\omega^2 \tau^2}{1 + \omega^2 \tau^2} - i \frac{\omega \tau}{1 + \omega^2 \tau^2} \right) \quad (3)$$

$$\mu = \mu_\infty \left(\frac{\omega^2 \tau^2}{1 + \omega^2 \tau^2} - i \frac{\omega \tau}{1 + \omega^2 \tau^2} \right) \quad (4)$$

where K_0 is the bulk modulus at the low frequency limit (corresponding to a liquid state); K_∞ and μ_∞ are respectively the bulk and the shear moduli of the material at the high frequency limit (corresponding to a solid state); ω is the angular frequency of the excitation signal; τ is the relaxation time.

Parameters K_0 , K_∞ and μ_∞ have been selected to match those of an epoxy resin [23]. Their values are displayed in Table 1.

Table 1: Elastic moduli of the viscoelastic interfacial medium

| K_0 | K_∞ | μ_∞ |
|---------|------------|--------------|
| 1.9 GPa | 3.6 GPa | 1.2 GPa |

The modification of the non-dimensional product parameter $\omega\tau$ makes it possible to change the mechanical properties of the interface layer. If we vary the value of this parameter from 0 to $+\infty$, the material constituting this layer can behave as an ideal fluid up to as a solid in regard to the propagating waves. Indeed, Figure 2 shows that the imaginary part of the shear modulus of the viscoelastic material is maximal for $\omega\tau = 1$. Below the value 1, the imaginary part clearly dominates the real one, which results in an exacerbated dissipation property of the interface layer, since the latter tends towards a liquid state. For values of $\omega\tau$ greater than 10 the shear modulus reaches a threshold equal to the value of the shear modulus of the material in its purely solid state. Thus, varying the value of this parameter makes it possible to simulate a degradation of the adherence quality which can be physically explained by the presence of defects such as delaminations [23].

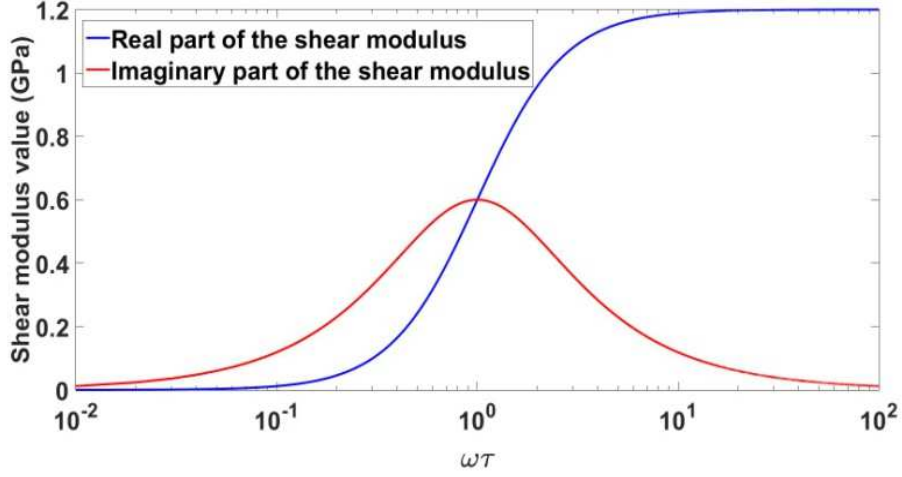


Figure 2: Evolution of the real and imaginary parts of the shear modulus μ with respect to the parameter $\omega\tau$

When writing the continuity conditions of displacements and stresses at the top and bottom interfaces with those of the surrounding fluid and using relations (1) and (2), one can obtain the expression of the reflection coefficient [24,25] as follows:

$$R = \frac{M_{11} - M_{22} - j(M_{21} \frac{\cos\theta_0}{\omega Z_0} + M_{12} \frac{\omega Z_0}{\cos\theta_0})}{-(M_{11} + M_{22}) + j(M_{12} \frac{\omega Z_0}{\cos\theta_0} - M_{21} \frac{\cos\theta_0}{\omega Z_0})} \quad (5)$$

where:

$$\begin{aligned} M_{11} &= T_{22}T_{41} - T_{21}T_{42} \\ M_{12} &= T_{23}T_{41} - T_{21}T_{43} \\ M_{21} &= T_{32}T_{41} - T_{31}T_{42} \\ M_{22} &= T_{32}T_{41} - T_{31}T_{42} \end{aligned} \quad (6)$$

$Z_0 = \rho_0 V_0$ is the acoustic impedance of the water surrounding the multilayer (with ρ_0 the density of water and V_0 the sound speed in water) and θ_0 the angle of incidence at which the wave penetrates in the studied multilayered structure.

In order to analyze the wave propagation inside the multilayered plates, the free guided waves dispersion curves have to be calculated. If we consider a multilayered structure surrounded by vacuum, it is possible to calculate the dispersion curves of the guided waves by adopting the free surfaces conditions. These conditions result in the following relation between the displacements and stresses located respectively at the bottom (referred to by the superscript bot) and the top (referred to by the superscript top) of the structure:

$$\begin{pmatrix} u_1^{\text{bot}} \\ u_3^{\text{bot}} \\ \sigma_{33}^{\text{bot}} \\ \sigma_{13}^{\text{bot}} \end{pmatrix} = \begin{pmatrix} T_{11} & T_{12} & T_{13} & T_{14} \\ T_{21} & T_{22} & T_{23} & T_{24} \\ T_{31} & T_{32} & T_{33} & T_{34} \\ T_{41} & T_{42} & T_{43} & T_{44} \end{pmatrix} \begin{pmatrix} u_1^{\text{top}} \\ u_3^{\text{top}} \\ \sigma_{33}^{\text{top}} \\ \sigma_{13}^{\text{top}} \end{pmatrix} \quad (7)$$

As we want to determine the free guided wave, corresponding to the multilayer structure surrounded by vacuum, it implies that the stress components σ_{33} and σ_{13} at the top and bottom interface of the multilayer have to be null.

Taking into account the nullity of the previous stress components, equation (7) possesses non trivial solutions only if:

$$\begin{vmatrix} T_{31} & T_{32} \\ T_{41} & T_{42} \end{vmatrix} = 0 \quad (8)$$

The numerical resolution of equation (8) allows, thus, to get the phase velocities of the free guided waves with respect to frequency. This equation can also be established by nullifying the denominator of the reflection coefficient, presented in the relation (5), and setting the parameter Z_0 to zero. Indeed, since the poles of the reflection coefficient correspond to the generalized guided waves radiating in the incident fluid environment ("leaky guided waves"), the free guided waves are obtained by setting the acoustic impedance, Z_0 , of the incident coupling fluid to zero, leading to equivalently determine the roots of the scalar value $M_{21} = 0$. The solutions of equation (8) are obtained numerically using the MATLAB® software. In our case, for each frequency, the phase velocities of the guided waves are derived via the process described above. These results are plotted, with respect to frequency, in order to build the dispersion curves of the free guided waves. This protocol provides accurate dispersion curves, even if some modes appear discontinuous due to the computation steps of the frequency and incident angle.

3. Reflection coefficient minima and free guided waves dispersion curves for a perfect interface

In Section 2, the methodology to obtain the reflection coefficient and the plate waves dispersion curves has been exposed.

The simulations were conducted on an aluminum/epoxy resin/steel multilayer structure as illustrated on Figure 3. It is considered in the rest of this paper as the reference trilayer. The adhesive layer bonding the aluminum and steel layers is much thinner than the thicknesses of the metallic layers in order to be considered as an interface layer. The material properties of the constituents [23,26] are displayed on Table 2.

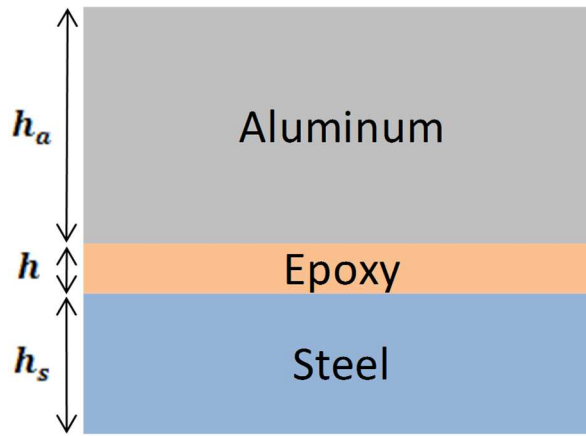


Figure 3: Isotropic multilayered structure: Aluminum / Epoxy resin / Steel, having respectively the thicknesses $h_a = 1.2$ mm, $h = 0.05$ mm and $h_s = 0.5$ mm

Table 2: Material properties of the isotropic multilayer

| Material | Aluminum | Epoxy resin | Steel |
|------------------------------|------------------------------|------------------------------|------------------------------|
| Velocities (m/s) | $C_1 = 6320$ $C_s = 3130$ | $C_1 = 2082$ $C_s = 1000$ | $C_1 = 5900$ $C_s = 3190$ |
| Density (kg/m ³) | 2700 | 1200 | 7800 |

In this Section, the validity of the calculation of the guided waves dispersion curves is compared to the results obtained via Finite Element (FE) method.

The equivalence between these curves and the reflection coefficient minima is then established when the impedance of the coupling fluid is negligible with respect to that of the solid materials. Finally, the guided modes coupling the three layers constituting the structure will be highlighted (*i.e.* the modes that propagate in the three layers).

a. Validity of the guided waves dispersion curves and their comparison with the reflection coefficient minima

In order to test our algorithm calculating the Lamb waves dispersion curves, numerical simulations are carried out using COMSOL Multiphysics® FEA software with the Solid Mechanics module. When using COMSOL, the trilayer sample is considered infinite along the x_1 and x_2 directions, in free boundary conditions and in vacuum. To this aim, a unit cell is meshed and Bloch-Floquet periodic boundary conditions are applied on its left and right sides. The Finite Element (FE) model is realized with a quadrangular regular mesh made of 2505 domain elements and 1022 boundary elements. An eigenfrequency parametric study is then performed where the wavenumber value $k_g = \frac{\omega}{c_\varphi}$ (c_φ being the guided wave phase velocity) is the sweep parameter.

The guided waves dispersion curves can be equivalently plotted displaying the phase velocity or the incidence angle with respect to the frequency. Indeed, according to the Snell's law, the incident angle θ_0 corresponding to each guided wave mode is given by:

$$\theta_0 = \arcsin\left(\frac{v_0}{c_\varphi}\right) \quad (9)$$

The representation displaying θ_0 with respect to the frequency facilitates the comparison between the reflection coefficient modulus $|R(\theta, f)|$ and the dispersion curves.

Figure 4 displays a comparison between the free guided waves dispersion curves calculated, using the reflection coefficient, via a MATLAB® algorithm, and the same dispersion curves calculated via COMSOL® following the process described above. A perfect agreement is denoted on this figure when comparing the curves obtained, for the structure described on Figure 3, through the theoretical model and the FE method for $0 \text{ MHz} < f < 9 \text{ MHz}$. Thus, it can be concluded that our algorithm calculating the guided waves dispersion curves in multilayered structures with perfect interface conditions provides satisfactory and reliable results.

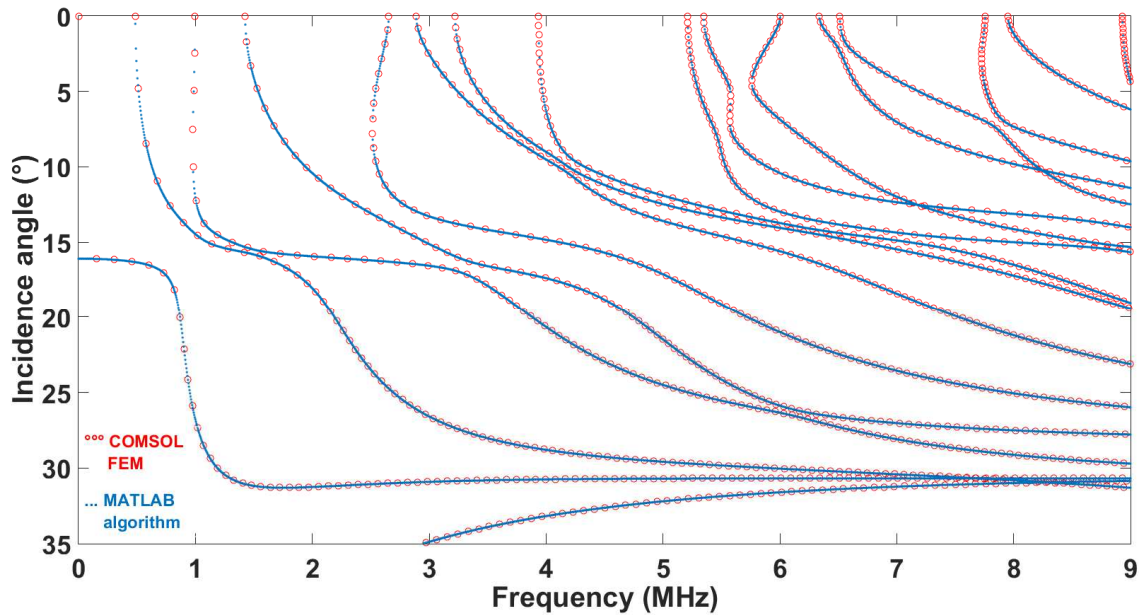


Figure 4: Comparison between the dispersion curves obtained by FE simulation on COMSOL® and by the MATLAB® algorithm for the reference trilayer

Figure 5 shows a comparison between the free guided waves dispersion curves, with respect to the incidence angle and the frequency, and the minima of the reflection coefficient obtained for this trilayer immersed in water within the frequency range 0 MHz - 9 MHz. The guided modes displayed on Figure 5 are pseudo symmetrical and pseudo anti-symmetrical because of the lack of a symmetrical plane in the structure [27] along the x_1 direction. In order to identify each propagation mode in the reference trilayer structure, the different modes will be simply labeled M_i with $0 < i < 16$ in the considered frequency range. The subscript i increases in the ascending order of the cutoff frequencies, except for M_0 and M_1 .

The black color corresponds to the minima of the reflection coefficient while the white color corresponds to the reflection coefficient equal to 1 in modulus. The reflection coefficient minima have excellent agreement with the free guided modes. Indeed, in most cases, the guided waves correspond to the minima of the reflection coefficient, when the coupling fluid density is small compared to the mass densities of the layers involved [27–29].

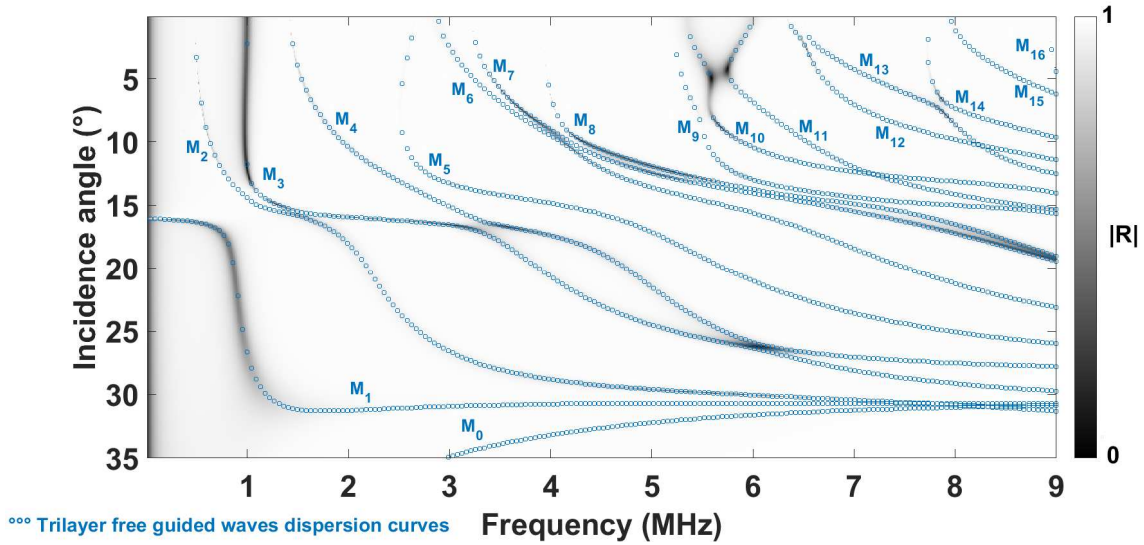


Figure 5: Comparison between reflection coefficient minima and guided waves dispersion curves plotted with respect to the incidence angle for the reference trilayer

When the assumption of a negligible impedance of the coupling fluid is made, the only guided mode that does not appear on the reflection coefficient minima is M_0 . In other words, this free guided mode does not have its equivalent in the resonance modes propagating in the trilayer structure.

b. Contribution of the different layers to the dispersion curves

An assumption was made that the guided waves dispersion curves calculated for the multilayer displayed on Figure 3 may consist in modes corresponding to the aluminum and steel layers taken separately and modes coupling those two layers via the adhesive layer of epoxy. This assumption is based on the fact that the impedance of the adhesive layer is largely inferior to those of the metallic ones. Because of this impedance discrepancy, some trilayer modes, at least for some frequency ranges, were expected to be mainly "trapped" in either the aluminum or the steel layer. The goal here is to identify the modes affected the most by the presence of the epoxy resin and hence, those that will be the most sensitive to the changes in the adherence quality.

In order to test this hypothesis, the free Lamb waves dispersion curves of the aluminum and steel layers are compared to the free guided waves in the trilayer. The dispersion curves of the trilayer are chosen here instead of the minima of the reflection coefficient for readability purposes only, since they are equivalent as it is shown on Figure 5.

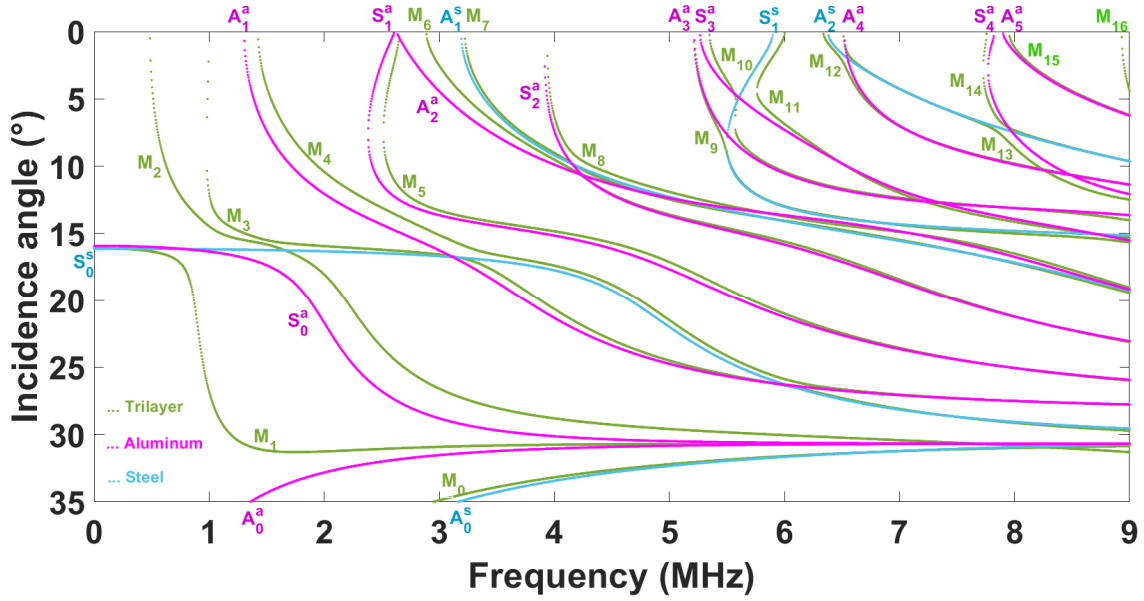


Figure 6: Comparison between the trilayer dispersion curves and the free Lamb modes of the aluminum and steel layers considered independently

For the aluminum and steel plates taken independently, and considering the frequency range of study, their antisymmetrical Lamb modes are named respectively A_i^a (with $0 < i < 5$) and A_i^s (with $0 < i < 2$) and the symmetrical ones are named S_i^a (with $0 < i < 4$) and S_i^s (with $i = 0; 1$).

Figure 6 shows that, as expected, the dispersion curves obtained for the trilayer structure possess many modes very close to those of the aluminum and steel layers, considered separately, and within particular frequency ranges. Indeed, these modes possess the same dispersive behavior as some Lamb modes propagating in the aluminum or steel plates. In order to determine the frequency extremities of the trilayer modes corresponding to Lamb modes propagating in the aluminum or steel layer, the following criterion have been observed: the limit for the incidence angle discrepancy, allowing to consider the modes as similar, has been set to 12.7 %. This maximum value has been chosen as it corresponds to the shift in incidence angle occurring between the M_2 and S_0^a modes (which have been considered as similar modes) at $f = 2.47$ MHz. It is to be noted, however, that in most cases, the discrepancy in incidence angle is much smaller than 12.7 %, and many modes are superimposed such as M_6 and S_2^a for $4.3 \text{ MHz} < f < 9 \text{ MHz}$.

Nevertheless, some modes do not fit any modes present in the layers taken independently from the multilayer. These modes are the most interesting when it comes to investigating the interface quality because they correspond to the multilayered structure and therefore to the effect of the adhesive layer.

The M_1 mode, which can be considered as a pseudo S_0 mode, propagating in the multilayer has a remarkable behavior that will be of great interest when the contact between the two metallic layers will be modified. Indeed, this mode is clearly a multilayer coupling mode especially for lower frequencies as it is visible on Figure 6 for a frequency range roughly located between 0.5 MHz and 3.5 MHz. This result corroborates the experimental and numerical results obtained by Balvantín *et al.* [16] who showed that within particular frequency ranges and applied load the propagation velocity of the S_0 mode is affected by the interfacial conditions.

It is noticeable that the clearest coupling modes (M_1, M_2, M_3) related to the global multilayered structure occur at low frequencies ($0.5 \text{ MHz} < f < 2 \text{ MHz}$). Since the wavelengths of the coupling modes are greater when the frequency decreases, the last ones become less sensitive to the individual layers, but more sensitive to the global multilayered structure.

A more detailed identification of the modes propagating in the trilayer structure is displayed on Table 3. Each mode propagating in the structure is either attributed to an aluminum or steel mode or to a coupling mode, depending on the frequency range. As noticed above, the coupling modes are those allowing to study the changes in interface quality because they depend strongly on the multilayered structure and therefore on the presence of the bonding layer between the two metallic ones.

Figure 6 shows also that the M_0 mode, which does not appear on the reflection coefficient minima, is very closely related to the steel Lamb mode A_0^s in the considered frequency interval. In that sense, M_0 is not relevant when it comes to assess the bonding interface quality because it is not a trilayer coupling mode. Thus, the fact that the M_0 mode does not appear in the reflection coefficient minima is not really limiting in the context of our study.

Table 3: Identification of the Lamb modes propagating in the trilayer structure with respect to the aluminum and steel layers as well as the coupling modes

| Trilayer modes | Aluminum layer modes and frequency ranges (MHz) | Steel layer modes and frequency ranges (MHz) | Coupling modes frequency ranges (MHz) |
|----------------|--|--|---------------------------------------|
| M_0 | | $A_0^s: 3 < f < 8.42$ | $8.42 < f < 9$ |
| M_1 | $A_0^a: 3 < f < 9$ | $S_0^s: 0 < f < 0.47$ | $0.47 < f < 3$ |
| M_2 | $S_0^a: 1.4 < f < 9$ | | $0.49 < f < 1.4$ |
| M_3 | $S_0^a: 3.27 < f < 6$ | $S_0^s: 2 < f < 3.27$ $S_0^s: 6 < f < 9$ | $1 < f < 2$ |
| M_4 | $A_1^a: 1.43 < f < 3.44$ $A_1^a: 6.2 < f < 9$ | $S_0^s: 3.44 < f < 6.2$ | |
| M_5 | $A_1^a: 2.6 < f < 9$ | | |
| M_6 | $A_2^a: 3.34 < f < 4.3$ $S_2^a: 4.3 < f < 9$ | | $2.9 < f < 3.34$ |
| M_7 | | $A_1^s: 3.22 < f < 9$ | |
| M_8 | $S_2^a: 3.9 < f < 4.2$ $A_2^a: 5.45 < f < 9$ | $A_1^s: 4.2 < f < 5.45$ | |
| M_9 | $A_3^a: 5.2 < f < 5.46$ $S_3^a: 8.7 < f < 9$ | $S_1^s: 5.46 < f < 8.7$ | |
| M_{10} | $S_3^a: 5.35 < f < 5.54$ $A_3^a: 5.7 < f < 9$ | | $5.54 < f < 5.7$ |
| M_{11} | $S_3^a: 5.76 < f < 8.65$ | $S_1^s: 5.76 < f < 6$ $S_1^s: 8.65 < f < 9$ | |
| M_{12} | $A_4^a: 6.5 < f < 9$ | $A_2^s: 6.34 < f < 6.5$ | |
| M_{13} | $A_4^a: 6.5 < f < 6.58$ $S_4^a: 7.8 < f < 9$ | $A_2^s: 6.58 < f < 7.8$ | |
| M_{14} | $S_4^a: 7.73 < f < 8$ | $A_2^s: 8 < f < 9$ | |
| M_{15} | $A_5^a: 7.95 < f < 9$ | | |
| M_{16} | | | $8.93 < f < 9$ |

As a conclusion, the guided modes propagating in the reference trilayer are composed of modes corresponding to the free Lamb waves of the aluminum or steel layers or coupling modes related to the global structure. Depending on the frequency ranges, these coupling modes parts are of the most interest in the following parts of our study since they provide information about the adherence quality between the metallic layers. These three types of modes are identified in Table 3.

4. Impact of different parameters of an adhesive joint

In the previous Section, the guided waves propagating in the reference trilayer have been labeled and some modes have shown to be more sensitive to the changes impacting the interface layer. In the current Section, the effect of different parameters of the adhesive layer on the reflection coefficient will be studied and compared with the free dispersion curves of the trilayer previously obtained.

a. Thickness of the adhesive layer

Figure 7 presents a comparison between the reflection coefficient calculated for the trilayer with two different thicknesses of the adhesive layer and the dispersion curves of the free guided waves of the reference structure defined in Figure 3 where the initial thickness of the adhesive layer is named h . The comparison has been done with thicknesses equal respectively to $h' = h/2$ and $h'' = 2h$.

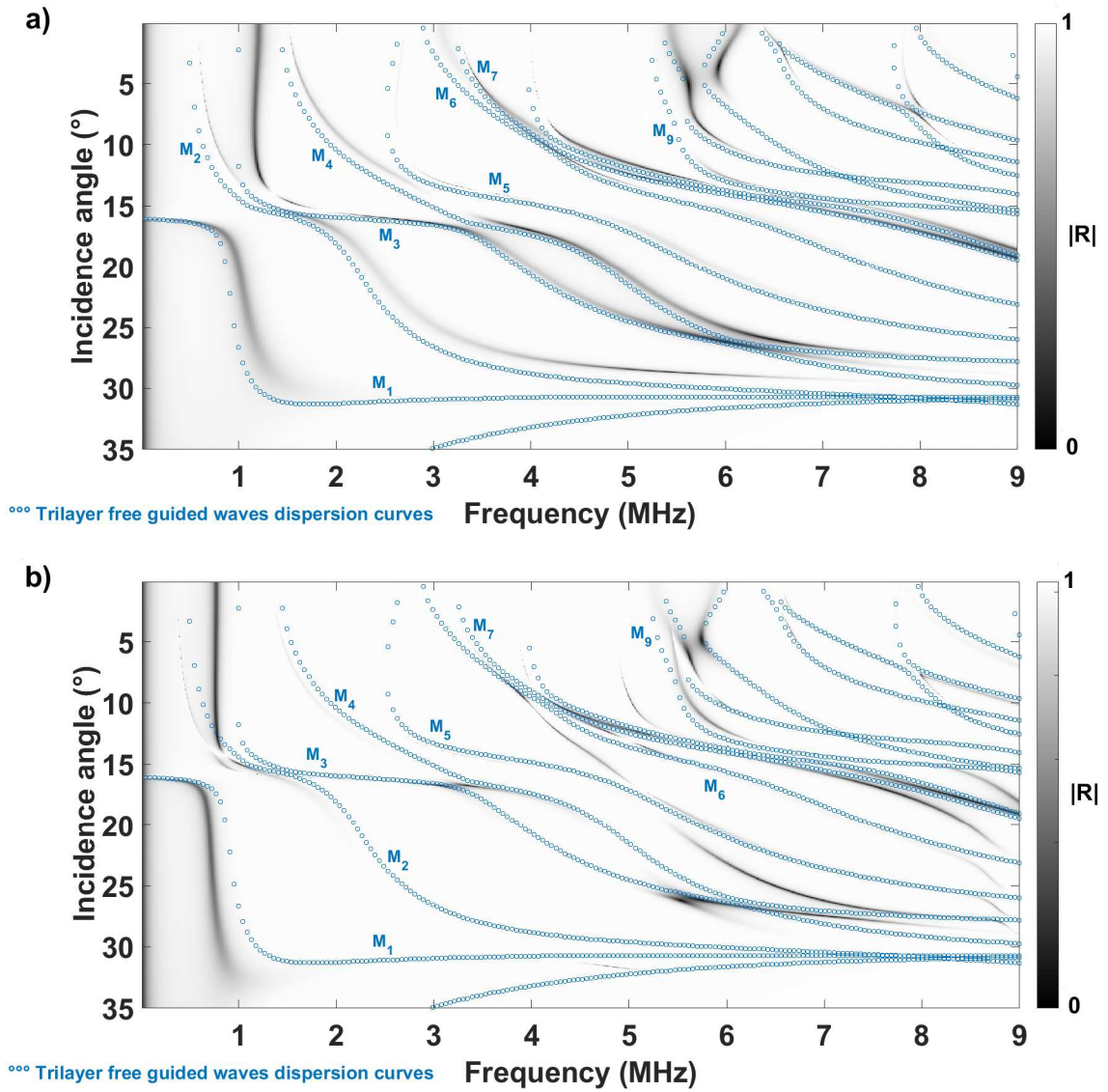


Figure 7: Comparison between the reflection coefficient calculated for the trilayer with different thicknesses of the adhesive layer and the free guided waves dispersion curves of the reference trilayer having an interface thickness h : a) $h' = \frac{h}{2}$ and b) $h'' = 2h$

First of all, Figure 7 shows that globally the discrepancy between the free guided waves dispersion curves and the reflection coefficient minima increase in the case of a greater thickness. For instance, some modes like M_2 and M_3 do not appear or appear only partially for $2 \text{ MHz} < f < 6 \text{ MHz}$ for the thicker interface layer when they are clearly represented for thinner one.

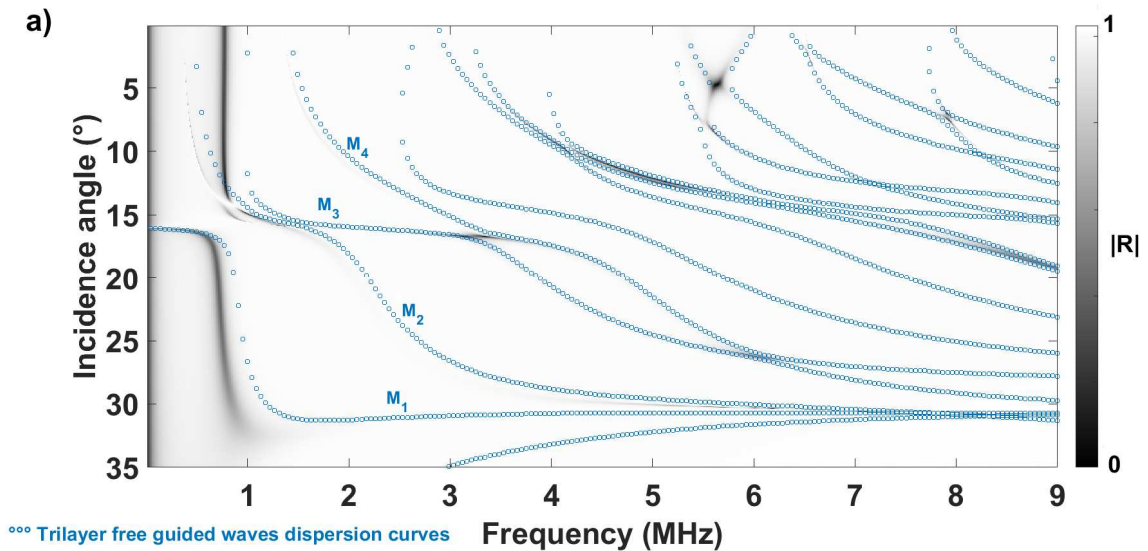
Shifts with respect to the dispersion curves do exist in both cases but they are accentuated in the case of $h'' = 2h$ as illustrated on M_4 mode for $5.4 \text{ MHz} < f < 7.1 \text{ MHz}$ or M_7 mode for $7.3 \text{ MHz} < f < 8.8 \text{ MHz}$. For the higher frequencies ($7.9 \text{ MHz} < f < 9 \text{ MHz}$), some minima of the reflection coefficient shift towards higher incidence angles which is equivalent to say that the modes M_4 , M_5 , M_6 , M_7 and M_9 propagate at lower velocities in the structure including a thicker adhesive layer. This behavior can be related to the increased effect of the thicker epoxy layer in which the wave velocities are inferior to those in the metals.

The minima corresponding to the trilayer coupling modes M_1 , M_2 and M_3 in the frequency range $0 \text{ MHz} < f < 1.7 \text{ MHz}$ are shifted when the thickness of the adhesive layer varies. This observation can be extended globally to all the coupling modes. When the thickness gets greater, these minima shift towards the lower frequencies and vice versa. This is in line with the fact that the smaller the thickness the higher the frequency must be in order to detect this interface layer.

To summarize, as could be expected, the discrepancies between the reflection coefficient minima and the guided waves dispersion curves of the reference trilayer structure increase when the thickness of the adhesive layer grows. For several modes, the phase velocities of the resonance modes of $|R|$ (modulus of the reflection coefficient) in the trilayer decrease when the thickness of the bonding layer increases. In addition, the position of the minima, with respect to the frequency, shift accordingly to the thickness of the interface layer, especially for the coupling modes M_1 , M_2 and M_3 . These results can be valuable for monitoring the thickness of an adhesive layer in a multilayer.

b. Density of the adhesive layer

The impact of the epoxy density is studied through a comparison (Figure 8) between the free guided waves dispersion curves of the reference trilayer (Figure 3) and the reflection coefficient minima of the multilayer structure with two different densities of the adhesive layer $\rho' = \rho/2$ and $\rho'' = 2\rho$, ρ being the initial density of the epoxy resin.



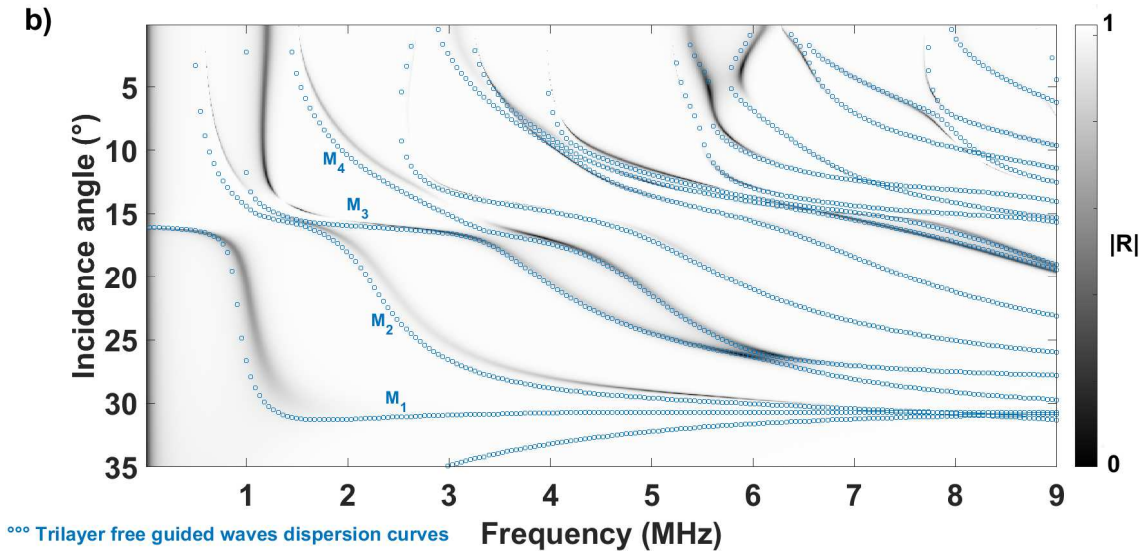


Figure 8: Comparison between the reflection coefficient calculated for the trilayer with two different densities of the adhesive layer and the free dispersion curves of the reference trilayer having an interface density ρ : a) $\rho' = \frac{\rho}{2}$ and b) $\rho'' = 2\rho$

When observing the reflection coefficient minima, the ρ' case generates less visible resonance modes than the ρ'' one. The decrease in density of the interface layer seems to lead to an increase of the reflection coefficient magnitude, therefore to a reduction of the number of minima which leads to a disappearance of some resonance modes in the trilayer. Indeed, when the density of the adhesive layer decreases, its impedance decreases too which leads to a greater reflection magnitude and prevents some resonance modes to propagate in the structure.

Conversely, the increase of the density of the interface layer causes an increase of the depth and width respectively of the peaks and valleys of the reflection coefficient. As it can be observed for several resonance modes such as those corresponding to M_2 in the frequency range $2 \text{ MHz} < f < 6 \text{ MHz}$ and M_4 in the frequency range $3.5 \text{ MHz} < f < 6 \text{ MHz}$, the width can be used as an index for determining some change in the density of the interface layer.

The minima of the reflection coefficient corresponding to the trilayer coupling modes M_1 , M_2 and M_3 in the frequency range $0 \text{ MHz} < f < 1.7 \text{ MHz}$ are shifted when the density of the adhesive layer varies. When the density grows, most of the resonance modes corresponding to coupling modes shift towards higher frequencies and conversely.

Another observation can be made: for the lower density (ρ') most of the resonance modes correspond globally more to the aluminum plate Lamb waves than to those of the steel plate as illustrated in Figure 9. This might be due to the fact that the reduced impedance of the adhesive layer tends to isolate the aluminum layer regarding the propagating waves. Exceptions can be observed for the minima corresponding to the modes S_0^s for $2.3 \text{ MHz} < f < 5.8 \text{ MHz}$, A_1^s for $3.4 \text{ MHz} < f < 4.1 \text{ MHz}$ and S_1^s for $5.5 \text{ MHz} < f < 5.8 \text{ MHz}$ that rather correspond to the free Lamb waves propagating in the bottom steel layer. These modes occur for lower frequencies which leads to think that the waves are more sensitive to the bottom layer for the greater values of the wavelength allowing to inspect a thicker portion of the trilayer.

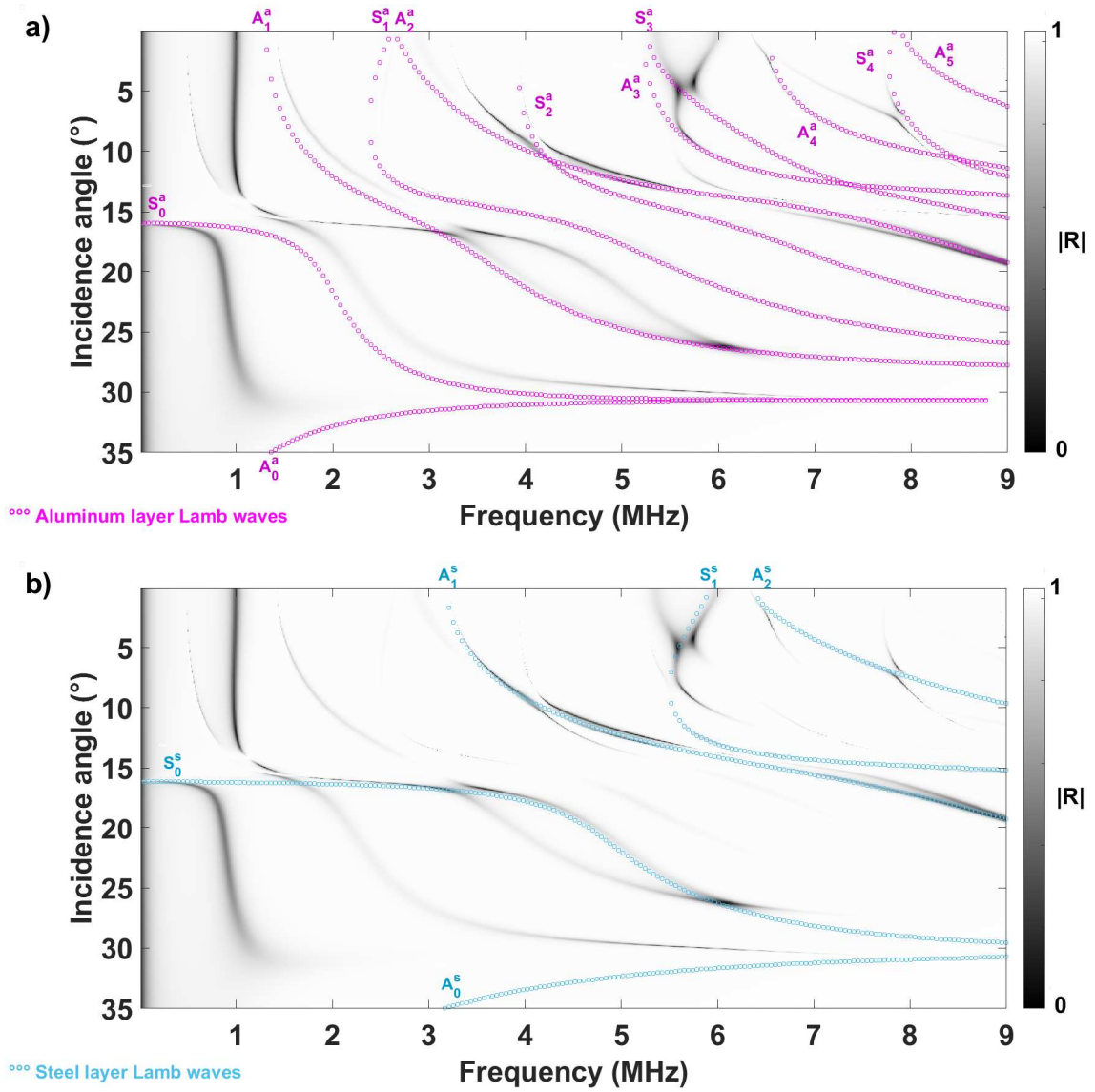


Figure 9: Comparison between the reflection coefficient of the trilayer containing an adhesive layer with a ρ' density and Lamb waves dispersion curves of the aluminum plate a) and steel plate b)

To summarize, when the density of the adhesive layer decreases, less resonance modes are generated in the structure because of the increased impedance discrepancy between the interface layer and the metallic ones. A better agreement is observed between the reflection coefficient minima and the upper layer free Lamb waves for a lower density of the interface layer. This behavior seems to be related to the "isolation" of the upper layer due to the reduced impedance of the bonding layer. Finally, the width and depth of several reflection coefficient minima can be used to monitor the adhesive layer density.

c. Viscoelastic interface layer model

The adhesive layer bonding the aluminum and steel layers is considered here as a viscoelastic interface layer. This model [1] assesses the interface quality through the value of the parameter $\omega\tau$. The simulations have been performed using the exact interface matrix given by Rokhlin *et al.* The exact interface matrix is chosen here because it can represent an actual adhesive layer. Indeed, this approach does not require the introduction of a very thin interface layer (with respect to the wavelength) synonymous of approximated interface matrices obtained after asymptotic expansions.

The reflection coefficient obtained for three values of $\omega\tau$ is compared to the free guided waves dispersion curves of the trilayer containing a perfect adhesive layer (Figure 10). The values chosen are: 0.1, 1, 10.

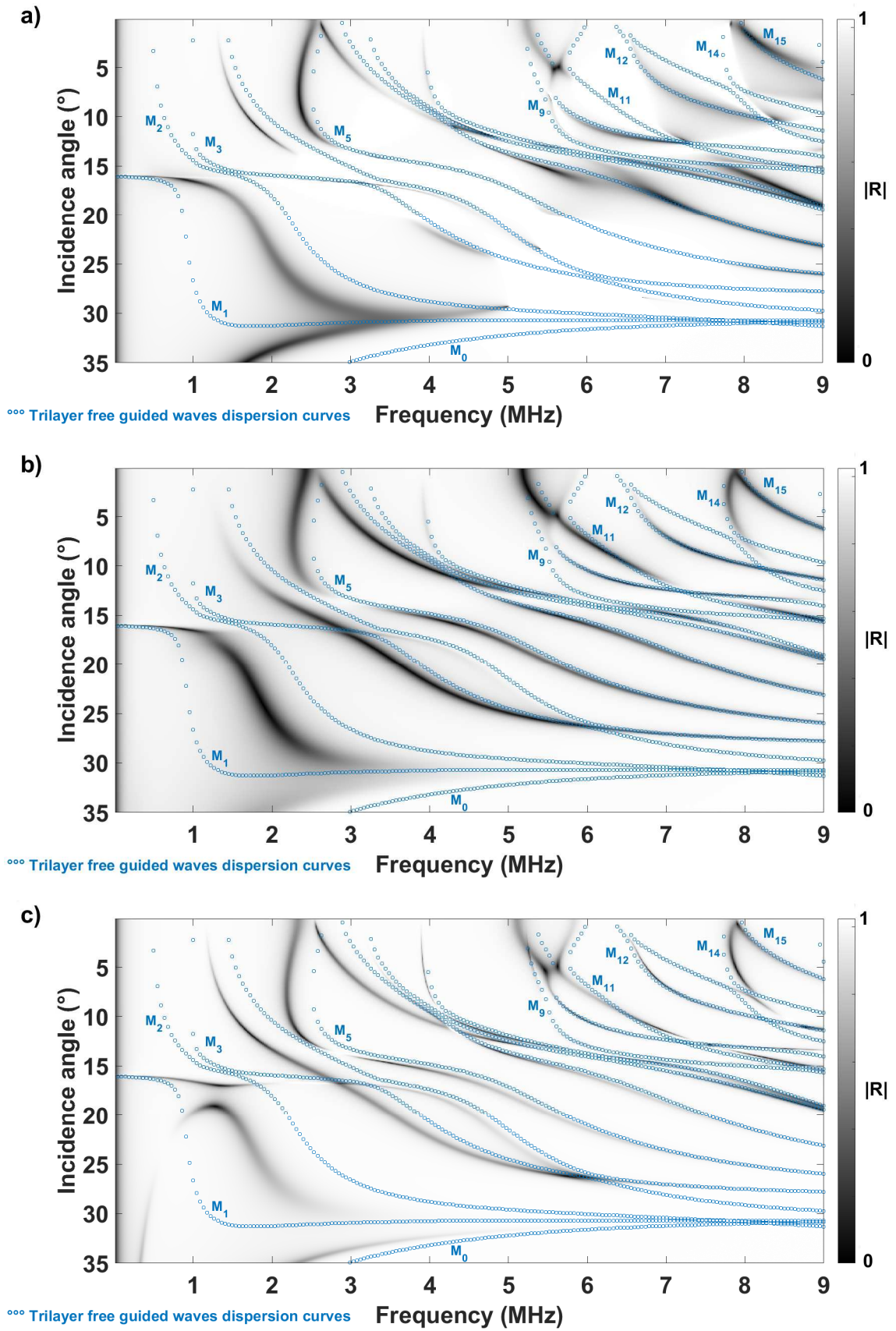


Figure 10: Comparison between the reflection coefficient calculated for the trilayer with different values of $\omega\tau$ for the interface layer and the free guided waves dispersion curves of the reference trilayer: a) $\omega\tau = 0.1$; b) $\omega\tau = 1$ and c) $\omega\tau = 10$

As shown on Figure 2, $\omega\tau = 0.1$ corresponds to an interface layer where the imaginary part of the shear modulus is dominant, $\omega\tau = 1$ to the case where the imaginary part is maximum but with an equivalent contribution of the real part, and finally $\omega\tau = 10$ to a state where the real part is largely predominant over the imaginary one and the shear modulus is very close to that of epoxy resin in its solid state.

From a practical point of view, $\omega\tau = 0.1$ represents a highly delaminated interface with a very strong influence of the induced fluid fraction on the wave propagation. The case where $\omega\tau = 1$ describes a moderately degraded adhesive layer with an important attenuation but insuring a reasonable transmission of shear displacement and stress. Finally, $\omega\tau = 10$ models a quasi perfect interface layer that possesses a shear modulus very close to that of a perfect solid epoxy layer.

For $\omega\tau = 0.1$, the agreement with the free guided waves dispersion curves is degraded compared to the higher values of $\omega\tau$. Indeed, some resonance modes such as M_5 for $3.4 \text{ MHz} < f < 5.5 \text{ MHz}$ and M_{11} for $5.8 \text{ MHz} < f < 6.9 \text{ MHz}$ are highly attenuated. Also, some extended minima areas connecting different resonance modes can be observed. For instance, M_{11} and M_{12} are connected between 6.9 MHz and 7.5 MHz and so are M_{14} and M_{15} between 8 MHz and 8.6 MHz. This behavior can be due to the fact that the reflection coefficient undergoes a strong attenuation for these resonance modes in these frequency ranges. Thus, it could be expected that these modes possess predominantly shear components since the imaginary part is dominant for $\omega\tau = 0.1$ as explained previously.

When $\omega\tau = 1$, the dissipative nature of the interface is maximum which leads to a spreading out of the minima areas (for example in the $1 \text{ MHz} < f < 3 \text{ MHz}$ range) and their deepening (shown by very dark color). The extension of the minima areas makes the discrimination of some very close modes impossible. Such a behavior can be observed for M_0, M_1 between 2.3 MHz and 4.3 MHz and for M_9, M_{10} between 5.2 MHz and 5.6 MHz. This is not observed when $\omega\tau = 0.1$ because, even though the dissipative nature of the interface is predominant, the imaginary part of the shear modulus is much lower than the maximum value reached for $\omega\tau = 1$.

The best agreement with the free waves dispersion curves is obtained for $\omega\tau = 10$. The example of the M_9 mode illustrates this. Indeed, the minimum of the reflection coefficient corresponding to this mode only appears for $\omega\tau = 10$. In addition, the minima are narrowest for this value of $\omega\tau$ which makes it easier to identify guided modes through comparison with the dispersion curves.

A remark must be made about the behavior of the M_2 and M_3 coupling modes in the frequency range $0.5 \text{ MHz} < f < 1.5 \text{ MHz}$: they do not seem to be generated for any of the $\omega\tau$ values considered here.

In summary, the quality of the interface between the two metallic layers can be modified via the value of $\omega\tau$ and the viscoelastic nature of the interface layer has clear effects on the reflection coefficient of the multilayer structure. Indeed, the higher the value of $\omega\tau$, the better the agreement with the free guided waves of the reference trilayer and the contribution of the viscoelastic dissipation, related to a delamination state, gets weaker and weaker. This can be a means to assess the quality of an interface and characterize the viscosity of an adhesive layer. Indeed, the results obtained here can be used to monitor the state of curing of an adhesive joint by evaluating its complex shear modulus through the value of $\omega\tau$ over time.

d. K_n and K_t parameters

In this Section, the K_n and K_t parameters [1,30] are taken into account in the interface layer transfer matrix in order to observe the influence of the parameter K_t on the reflection coefficient. K_n and K_t are respectively the normal and transverse stiffnesses of the interface layer and have dimensions N/m^3 . This approach allows to assess the interface quality in a straightforward and simple way. Indeed, in practical cases a delamination introduces a fluid fraction in the interface layer, so varying the value of K_t makes sense in order to quantify the amount of shear stress transmitting through the interface. The goal here is also to assess the relevance of the K_n/K_t approach in the studied configuration. The stiffnesses K_n and K_t are defined by:

$$K_n = \frac{\Lambda_i + 2\mu_i}{h} \quad (10)$$

$$K_t = \frac{\mu_i}{h} \quad (11)$$

where Λ_i and μ_i are the Lamé constants of the interfacial medium.

To extract K_n and K_t from respectively the component B_{23} and B_{14} of the interface layer matrix given by Rokhlin *et al.* [1], a first order approximation has to be performed assuming that λ_0 (the longitudinal wavelength in the interface layer) is much greater than the thickness h of the interface layer.

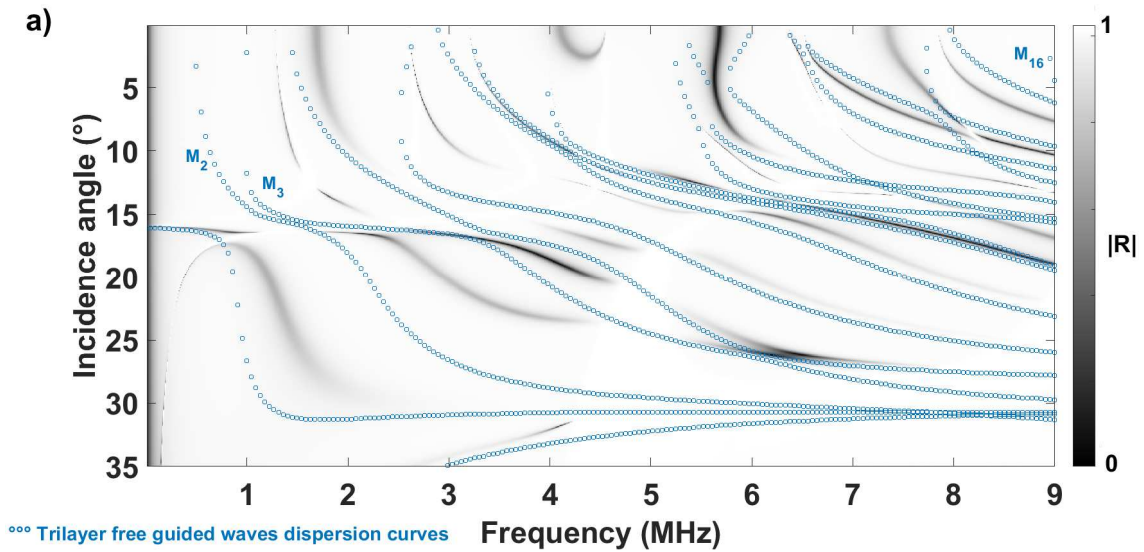
In the present study, the transfer matrix components are kept identical but now the longitudinal and transverse waves velocities are recalculated with respect to the Lamé constants. Considering the equations (9) and (10), the Lamé constants vary depending on the values of K_n , K_t and h of the studied cases.

The value of K_n is here set to 10^{15} N/m³ which insures a good transmission of the normal stress. The higher the value of K_t , the better the contact between the two metals will be.

Figure 11 is a comparison between the reflection coefficient computed for the values $5 \cdot 10^{12}$ N/m³ and 10^{15} N/m³ of the parameter K_t , representing respectively a highly altered interface and a good quality interface, and the free guided waves dispersion curves obtained for the reference trilayer (Figure 3).

This comparison shows that a low value of K_t leads, as expected, to a poor agreement with the free plate waves dispersion curves. Indeed, some resonance modes are only partially generated (highly attenuated) such as those corresponding to M_2 ($1.7 \text{ MHz} < f < 4.3 \text{ MHz}$) and M_3 ($2.6 \text{ MHz} < f < 4.6 \text{ MHz}$). Some other resonance modes are not excited like the modes which correspond to M_{16} and M_2 for $0.5 \text{ MHz} < f < 1.7 \text{ MHz}$ to the contrary of the case with $K_t = 10^{15}$ N/m³. These modes are quite specific because they are trilayer coupling modes directly related to the presence of the adhesive layer. In that regard, a small value of K_t leads to the non-generation of some coupling modes. These very attenuated resonance coupling modes appear to be mainly shear modes because of the strong influence that a low value of K_t (or μ_i) has upon them.

However, for higher values of K_t , a much better agreement is expected. Indeed, the minima shifts with respect to the dispersion curves are quite significant. Such a behavior might be due to the ratio $\beta = \frac{h}{\lambda_0}$ that gets too small for the most part of the considered frequencies. Indeed, this ratio varies linearly from 0 to 0.22 for $f = 9 \text{ MHz}$, which seems too small in the context of the K_n/K_t approach which necessitates a much higher ratio allowing to neglect the inertia of the interface layer [1].



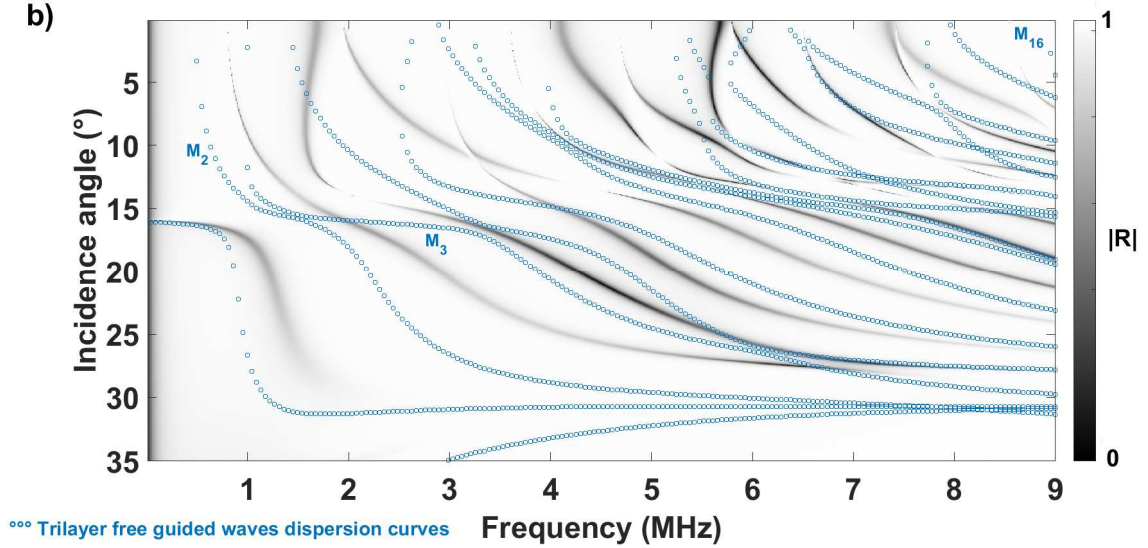


Figure 11: Comparison between the reflection coefficient calculated for two different values of K_t and the free guided waves dispersion curves of the reference trilayer: a) $K_t = 5 * 10^{12} \text{ N/m}^3$ and b) $K_t = 10^{15} \text{ N/m}^3$

Finally, the K_n/K_t approach is shown to be a qualitative tool allowing to assess, in a coherent way, the adherence quality within a multilayered structure despite some limitations due to the thickness of the adhesive layer. One of the interesting and noticeable effects of a low value of K_t is the high attenuation of shear coupling modes. The K_n/K_t approach does not affect the value of Λ_i , maintained constantly at a value insuring a very high K_n , but focuses only on the value of μ_i which allows to vary the value of the transverse stiffness of the adhesive layer, which can be directly related to the bonding quality. The K_n/K_t approach presented in this study is a way to quantify the adherence quality through the transverse stiffness value, which can be related directly to the shear velocity and therefore the transverse acoustic impedance.

5 Conclusion and future work

In this work, the effect on ultrasonic guided waves of the properties of different interface layers is numerically studied in the context of a multilayered structure. Reflection coefficients and free guided waves dispersion curves are modeled using the global transfer matrix method. The characterization of variable properties of the adhesive layer by means of a comparison with free guided waves dispersion curves of the trilayer containing a perfect epoxy layer is proposed.

An isotropic multilayered system consisting of aluminum, epoxy resin and steel is the configuration studied in this work. The equivalence between the reflection coefficient magnitude minima and the free guided waves dispersion curves has been established for the considered structure. Multilayer coupling modes have been highlighted through a comparison between the free guided waves dispersion curves of the trilayer and the free Lamb waves of the aluminum and steel plates respectively. Then, the impact of the thickness and density of the adhesive layer has been studied with respect to the guided modes, especially with regard to the coupling modes that are the most sensitive to the changes in the interface layer.

Imperfect interface layer models have also been implemented. These models assess the interface quality through a viscoelastic parameter $\omega\tau$ and the normal and transverse interface stiffnesses K_n and K_t . The increase of $\omega\tau$ results in a better interface quality and a much better agreement with the free guided waves of the reference trilayer. Regarding the K_n/K_t approach, K_n is set at a high value insuring a good transmission of the normal stress and two extreme values of K_t are tested. A very high value of K_t provides reflection coefficient minima much closer to the free guided waves dispersion curves of the reference trilayer structure, however the agreement is not as good as expected. This behavior might be due to the thickness of the interface layer which is too large with respect to the wavelengths generated in the medium.

This study provides an overview of the impact of the adhesive interface layer nature on the reflection coefficient magnitude and the potential of the comparison with the free guided waves dispersion curves in order to characterize the interface quality within a multilayered structure.

Thus, it could be envisaged to characterize interface defects through experimental $V(z,f)$ measurements. For this, the reflection coefficients obtained by modeling should be compared to the experimental ones rebuilt thanks to the inversion of measured $V(z,f)$ data. Such a study is currently being initiated.

Acknowledgement

This work has been supported by the co-labeled EURIPIDES² and CATRENE project SAM³ (Smart Analysis Methods for 3D Integration).

References

- [1] S.I. Rokhlin, Y.J. Wang, Analysis of boundary conditions for elastic wave interaction with an interface between two solids, *J. Acoust. Soc. Am.* 89 (1991) 503–515.
- [2] J.-M. Baik, R.B. Thompson, Ultrasonic scattering from imperfect interfaces: A quasi-static model, *J. Nondestruct. Eval.* 4 (1984) 177–196.
- [3] D. Jiao, J.L. Rose, An ultrasonic interface layer model for bond evaluation, *J. Adhes. Sci. Technol.* 5 (1991) 631–646.
- [4] P.P. Delsanto, M. Scalerandi, A spring model for the simulation of the propagation of ultrasonic pulses through imperfect contact interfaces, *J. Acoust. Soc. Am.* 104 (1998) 2584–2591.
- [5] Y.A. Antipov, O. Avila-Pozos, S.T. Kolaczowski, A.B. Movchan, Mathematical model of delamination cracks on imperfect interfaces, *Int. J. Solids Struct.* 38 (2001) 6665–6697.
- [6] S.I. Rokhlin, W. Huang, Ultrasonic wave interaction with a thin anisotropic layer between two anisotropic solids: Exact and asymptotic-boundary-condition methods, *J. Acoust. Soc. Am.* 92 (1992) 1729–1742.
- [7] A. Boström, G. Wickham, On the boundary conditions for ultrasonic transmission by partially closed cracks, *J. Nondestruct. Eval.* 10 (1991) 139–149.
- [8] M. V Golub, Propagation of elastic waves in layered composites with microdefect concentration zones and their simulation with spring boundary conditions, *Acoust. Phys.* 56 (2010) 848–855.
- [9] A. Boström, M. Golub, Elastic SH wave propagation in a layered anisotropic plate with interface damage modelled by spring boundary conditions, *Q. J. Mech. Appl. Math.* 62 (2009) 39–52.
- [10] A. Pilarski, J.L. Rose, A transverse wave ultrasonic oblique incidence technique for interfacial weakness detection in adhesive bonds, *J. Appl. Phys.* 63 (1988) 300–307.
- [11] P. Fraisse, F. Schmit, A. Zarembowitch, Ultrasonic inspection of very thin adhesive layers, *J. Appl. Phys.* 72 (1992) 3264–3271.
- [12] P.B. Nagy, Ultrasonic classification of imperfect interfaces, *J. Nondestruct. Eval.* 11 (1992) 127–139.
- [13] B. Drinkwater, R. Dwyer-Joyce, P. Cawley, A study of the transmission of ultrasound across solid–rubber interfaces, *J. Acoust. Soc. Am.* 101 (1997) 970–981.
- [14] S. Mustapha, L. Ye, Propagation behaviour of guided waves in tapered sandwich structures and debonding identification using time reversal, *Wave Motion.* 57 (2015) 154–170.
- [15] R. Leiderman, A.M.B. Braga, Scattering of guided waves by defective adhesive bonds in multilayer anisotropic plates, *Wave Motion.* 74 (2017) 93–104.
- [16] A.J. Balvantín, J.A. Diosdado-De-la-Peña, P.A. Limon-Leyva, E. Hernández-Rodríguez, Study of guided wave propagation on a plate between two solid bodies with imperfect contact conditions, *Ultrasonics.* 83 (2018) 137–145.
- [17] R. Leiderman, J.C. Figueroa, A.M.B. Braga, F.A. Rochinha, Scattering of ultrasonic guided waves by heterogeneous interfaces in elastic multi-layered structures, *Wave Motion.* 63 (2016) 68–82.
- [18] N. Guo, P. Cawley, The interaction of Lamb waves with delaminations in composite laminates, *J. Acoust. Soc. Am.* 94 (1993) 2240–2246.
- [19] A. Pilarski, J.L. Rose, J. Ditri, D. Jiao, K. Rajana, Lamb Wave Mode Selection for Increased Sensitivity to Interfacial Weaknesses of Adhesive Bonds BT - Review of Progress in Quantitative Nondestructive Evaluation: Volumes 12A and 12B, in: D.O. Thompson, D.E. Chimenti (Eds.), Springer US, Boston, MA, 1993: pp. 1579–1585.
- [20] L. Singher, Y. Segal, E. Segal, J. Shamir, Considerations in bond strength evaluation by ultrasonic guided waves, *J. Acoust. Soc. Am.* 96 (1994) 2497–2505.
- [21] P. Karpur, T. Kundu, J.J. Ditri, Adhesive Joint Evaluation Using Lamb Wave Modes with Appropriate Displacement, Stress, and Energy Distribution Profiles BT - Review of Progress in Quantitative Nondestructive Evaluation: Volume 18A–18B, in: D.O. Thompson, D.E. Chimenti (Eds.), Springer US, Boston, MA, 1999: pp. 1533–1542.
- [22] L.M. Brekhovskikh, *Waves in layered media*, Academic Press, 1960.
- [23] A.I. Lavrentyev, S.I. Rokhlin, Models for ultrasonic characterization of environmental degradation of interfaces in adhesive joints, *J. Appl. Phys.* 76 (1994) 4643–4650.
- [24] M. Lematre, Y. Benmehrez, G. Bourse, J.W. Xu, M. Ourak, Acoustic microscopy measurement of elastic constants by using an optimization method on measured and calculated SAW velocities: effect of

- initial c_{ij} values on the calculation convergence and influence of the LFI transducer parameters on the determination of the SAW velocity, *NDT E Int.* 35 (2002) 279–286.
- [25] M. Lematre, Y. Benmehrez, G. Bourse, J.W. Xu, M. Ourak, Determination of elastic parameters in isotropic plates by using acoustic microscopy measurements and an optimization method, *NDT E Int.* 35 (2002) 493–502.
- [26] A. Demcenko, L. Mazeika, Calculation of Lamb waves dispersion curves in multi-layered planar structures, *ULTRAGARSAS Ultrasound.* (2002).
- [27] Y.-C. Lee, S.-W. Cheng, Measuring Lamb wave dispersion curves of a bi-layered plate and its application on material characterization of coating, *IEEE Trans. Ultrason. Ferroelectr. Freq. Control.* 48 (2001) 830–837.
- [28] S.I. Rokhlin, Recent advances in waves in layered media, *J. Phys.* (1992).
- [29] M.J.S. Lowe, P. Cawley, The applicability of plate wave techniques for the inspection of adhesive and diffusion bonded joints, *J. Nondestruct. Eval.* 13 (1994) 185–200.
- [30] M. Schoenberg, Elastic wave behavior across linear slip interfaces, *J. Acoust. Soc. Am.* 68 (1980) 1516–1521.